Laser Welding of Thin Copper and Aluminum Sheets: Feasibility and Challenges in Continuous-Wave Welding of Dissimilar Metals

A. Fortunato [1] · A. Ascari [1] (ORCID)

Abstract

The present paper defines process windows for laser welding of thin copper and aluminum sheets in Al-Cu and Cu-Al lap-joint configurations, exploiting different process strategies and parameters. A single-mode continuous-wave (CW) laser source was exploited with both linear and wobbling strategies. In both cases the influence of several parameters, such as, laser power, spot dimensions and scanning speed on the resulting microstructure and joint strength was analyzed. The influence of one, two and three parallel beads on the maximum shear strength was also evaluated. The optimum process configurations were finally determined based on maximum joint strength in shear tests and the mixing of the two parent metals occurring after welding was determined by means of SEM-EDS analysis.

Keywords Laser welding · Dissimilar welding · High reflectivity materials · Copper · Aluminum

Introduction

Welding of dissimilar materials has been studied and optimized throughout the last decades in order to meet the increasing demands in performance characterizing modern industrial production. The need, in fact, to optimize industrial products in terms of mass, stiffness, strength and resistance to corrosion and/or high temperatures, pushed manufacturing technologies towards the possibility to deal with hybrid, composite and dissimilar materials. In particular, the possibility to join different metallic materials together, by means of traditional and new joining techniques, represents an important step towards new manufacturing solutions. The first studies in this direction were

✉ A. Ascari
a.ascari@unibo.it

1 Department of Industrial Engineering, University of Bologna, Viale Risorgimento 2, 40136 Bologna, Italy

conducted in aluminum to steel welding. Initially the main efforts were devoted to solid state welding, since it allows a very low dilution between the two materials and determines a low thermal degradation, thanks to the absence of a fused zone: solid state pressure welding [1], impact welding [2], friction stir welding [3] and friction stir welding [4]. The constraints in geometry of the workpiece and in joint type imposed by those joining techniques, then, pushed the researchers towards autogenous welding: in particular laser welding immediately proved itself to be a promising technology thanks to its low heat input and fine-tunability [5]. Besides the aluminum/steel combination, aluminum/copper dissimilar welding also turned out to be of great industrial interest, especially for electronic, optoelectronic and automotive industry. The first studies immediately pointed out how the accurate and controllable heat input typical of laser welding was crucial for keeping the interaction between the two metals very low and thus reducing the formation of brittle and hard intermetallic phases [6]. The problem of intermetallics had already been pointed out in [7], where the authors stressed on their growth in case of cold roll welding, and in [8], where the authors pointed out that a large formation of intermetallics leads to a low electrical conductivity of the joint. The efforts, throughout the years, towards the study of Al/Cu dissimilar welding involved various techniques: friction stir welding [9], friction welding [10], hybrid laser-friction stir welding [11], magnetic pulse welding [12] and ultrasonic welding [13]. All the mentioned scientific contributions stress on the importance of setting up a joining technique which determines the lowest amount of intermetallics in the joint, in order to maximize both mechanical behavior and electrical conductivity. Concerning autogenous welding of dissimilar Al-Cu configurations, laser techniques play a dominant role and in the last five years many efforts were devoted to assessing the feasibility of the process with respect to the different parameters and to the various laser sources applicable. In [14] Weigl et al. exploited an AlSi12 pre-placed filler wire in butt laser welding of 1 mm thick aluminum and copper plates. The high silicon content of the wire proved to be favorable to the limitation of intermetallics formation. In [15] Solchenbach et al. conducted a study on lap welding of 0.5 mm thick foils of aluminum on 0.5 mm thick foils of copper exploiting a 400 W modulated laser and a galvo scanner. The weld beads were obtained using the wobbling technique in order to enlarge the melt pool and favor a brazing of aluminum on copper in order to hinder the formation of intermetallics. In [16] Lee et al. performed a study concerning the application of a high brilliance single mode 2.0 kW fiber laser and a fixed focal head in lap welding of 0.3 mm thick aluminum on copper and copper on aluminum. In this case the extremely high power density available allowed a very high welding speed (up to 50 m/min) and a very low heat input, valid for keeping the formation of intermetallics very low and achieving sound joints in both configurations. In [17] Zuo et al. performed a lap welding of 0.3 mm thick copper on 0.3 mm thick aluminum sheets with a low brilliance Nd:YAG laser and a fixed focal head. They pointed out the role of the different intermetallics on the mechanical performance of the joints, pointing out that the most brittle phase is θ-CuAl$_2$. In [18] Stritt et al. pointed out that a proper pulse shaping promotes the right mixing of the liquid phases in aluminum over copper pulsed laser lap welding. In [19] Fetzer et al. exploited a 4.0 kW diode laser source and a galvo scanner in lap welding 1 mm thick aluminum on copper. The results pointed out the benefits of performing a beam oscillation during welding in order to enlarge and evenly distribute the melt-pool. In [20] Schmalen et al. carried out an investigation on lap welding of 0.5 mm thick plates of aluminum on copper exploiting a disk laser, equipped with a galvo scanner, and a beam oscillating

technique. The authors identified that most cracks propagate in the interface between η_2 and γ_1 phases. In [21] Reisgen et al. performed butt welding of 2 mm thick aluminum and copper plates exploiting a single mode 2.0 kW fiber laser and beam oscillation in a vacuum chamber. The results were characterized in terms of electrical resistance and the best solution was to exploit a 0.3 mm offset of the laser beam in the aluminum side. In [22] Kermanidis et al. investigate long pulse laser spot welding of copper tubes on aluminum foils. The results pointed out, also in this case, that the formation of intermetallics is directly dependant on the heat input. Considering the literature review proposed, it is clear that Al-Cu dissimilar welding is a very hot topic and that laser autogenous welding, in particular, plays a fundamental role as one of the top candidates for future industrial applications. According to these considerations the present paper involves a continuous wave 1.0 kW single mode fiber laser and a galvo scanner in lap welding of Al and Cu thin foils. This configuration has proven, in fact, to be the best performer in terms of welding speed and versatility and it can be used both in linear and wobbling (oscillating beam) configuration. The experimental campaign carried out was aimed at overviewing any possible welding configuration, taking into account Al-Cu and Cu-Al lap joints, proximity and remote welding (with the exploitation of two different focal lengths of the F-Theta lens: 160 mm and 420 mm), linear and wobbling strategy. The results were characterized in terms of depth and width of the weld bead, mechanical shear testing and EDX composition analysis of the fused zone.

Experimental Setup

All experiments were carried out on commercially pure copper (Cu > 99.6%), coated with a thin nickel layer in order to improve optical absorptivity of the laser radiation and to avoid surface oxidation, and commercially pure aluminium AA1060 (99.4% Al, 0.25% Si and 0.35% Fe). All samples consisted of 80 × 45 foils with nominal thickness of 0.3 mm for the copper alloy and 0.4 mm for the aluminum one, welded in a lap-joint configuration as shown in Fig. 1. Geometric parameters considered for characterization of the weld beads are shown in Fig. 2, while the physical properties of both materials are reported in Table 1.

For all tested process parameters, both Al-Cu and Cu-Al configurations were investigated, in order to understand the importance of laser absorption and melt pool dynamics during re-solidification.

An IPG YLR-1000-SM single-mode fiber laser with a maximum power output of 1 kW, wavelength of 1070 nm and BPP of 0.4 mm·mrad was utilized for experiments. The core of the delivery fiber was 14 μm in diameter and the collimator focal length
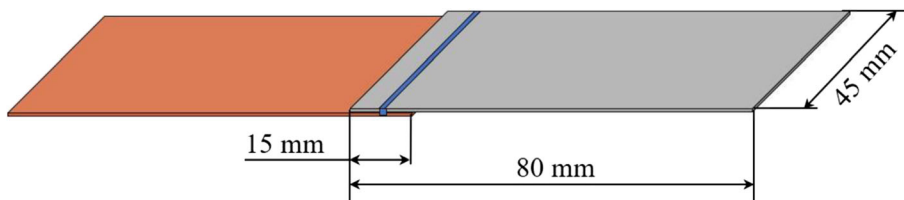

15 mm   80 mm   45 mm

Fig. 1 Joint configuration
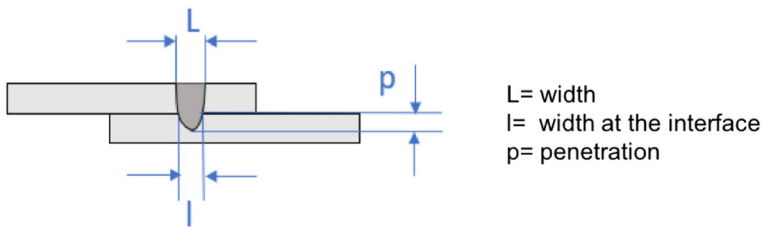
L= width
l= width at the interface
p= penetration

Fig. 2 Definition of geometric parameters

was 100 mm. As mentioned in the introduction, two different focal lengths were employed for tests. These consisted of a 160 mm focusing F-Theta lens, which produced a theoretical spot diameter of 22.4 μm and a maximum power density of 253.8 MW/cm^2, and a 420 mm focusing F-Theta lens, which produced a theoretical spot diameter of 58.8 μm and a maximum power density of 36.8 MW/cm^2. Laser beam displacement was achieved by means of a SmartMove SH20G-XY2 galvo scanning head. Both linear and wobbling techniques were involved in the tests and the full experimental campaign is described in Tables 2 and 3. The different levels of the process parameters were chosen carrying out a preliminary experimental campaign.

The wobbling strategy was implemented by programming the galvo head so that the actual laser beam path was the result of the superimposition of a circular motion and of a linear one, as shown in Fig. 3 (top).

The beam rotates along a circle with a diameter equal to the wobbling thickness t_h at a tangential speed V_t. The center of the circular path is moved along the welding direction at a constant speed V_f so that two subsequent revolutions are overlapped one another of a fixed quantity $O_\%$. The mathematical formulas governing this combined motion are shown in eq. 1.

$$\begin{cases} x(t) = \dfrac{t_h}{2}\cos\left(\dfrac{2V_t}{t_h}t\right) + V_f t \\ y(t) = \dfrac{t_h}{2}\sin\left(\dfrac{2V_t}{t_h}t\right) \end{cases} \quad (1)$$

According to these considerations the actual beam path is a cycloid similar to the one shown in Fig. 3 (bottom). The equipment used in the experimental activity described

Table 1 Physical properties of aluminum and copper

	Copper	Aluminum
Density	8.9 g/cm^3	2.71 g/cm^3
Melting temperature	1083 °C	660 °C
Thermal conductivity	390 W/(m·K)	226 W/(m·K)
Thermal expansion coefficient	17·10^{-6} °C^{-1}	24·10^{-6} °C^{-1}
Specific heat capacity	385 J/(kg·K)	880 J/(kg·K)

Table 2 Process parameters investigated for linear scanning strategy

Linear	Focal length (F) [mm]	Spot diameter [μm]	Laser power (P) [W]	Welding speed (V_f) [mm/s]
Test A (Al-Cu)	160	22.4	500-750-1000	200–450-700
Test B (Al-Cu)	420	58.8	500-750-1000	100–300-500
Test E (Cu-Al)	160	22.4	500-750-1000	100–350-600
Test F (Cu-Al)	420	58.8	800–900-1000	100–350-400

herein was programmed in terms of wobbling thickness (t_h), overlapping ($O_\%$) and tangential speed (V_t): by means of eq. 2 and 3 these parameters can easily be turned into a wobbling frequency (f) and a welding speed (V_f). The complete resume of all the exploited wobbling parameters is shown in Tables 3 and 4.

$$f = \frac{V_t}{\pi t_h} \qquad (2)$$

$$V_f = f\left(t_h - \left(\frac{t_h O_\%}{100}\right)\right) \qquad (3)$$

In order to evaluate the influence of multiple weld beads on the maximum strength, single, double and triple weld beads were carried out with a pitch of 3 mm. In each case, the range of process parameters considered for the experiments was determined basing on preliminary tests. The whole experimental campaign consisted of 700 weldments.

The interface zones of each Al-Cu and Cu-Al joint were analysed via Scanning Electron Microscopy (SEM) and Energy Dispersive X-ray Spectroscopy (EDS) for evaluation of the chemical composition after re-solidification. Welded joint strength was measured for significant samples via shear tests at a speed of 0.025 mm/s.

Results and Discussion

Morphology and Microstructure in Welding with Linear Scanning Strategy

Figures 4 and 5 show the evolution of weld bead penetration depth and width with respect to the varied process parameters both in Al-Cu and Cu-Al configurations when

Table 3 Process parameters investigated for wobbling scanning strategy

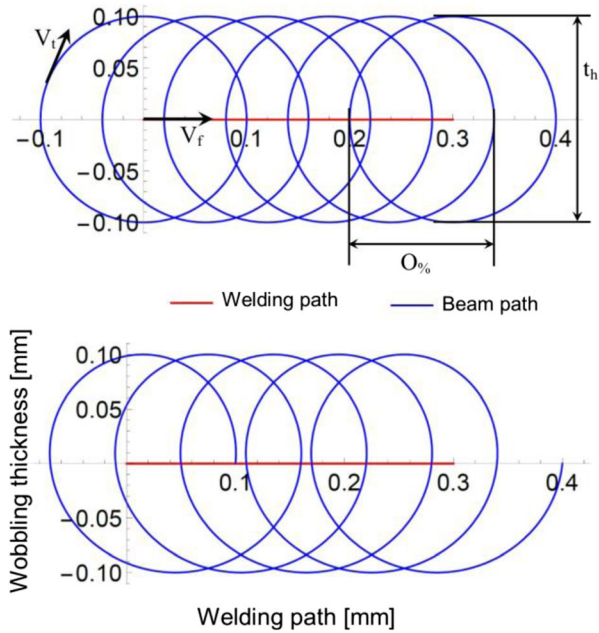| Wobbling	Focal length (F) [mm]	Spot diameter [μm]	Laser power (P) [W]	Tangential speed (V_t) [mm/s]	Wobbling thickness (t_h) [mm]
Test C (Al-Cu)	160	22.4	500-750-1000	150–375-600	0.1–0.2
Test D (Al-Cu)	420	58.8	500-750-1000	100–350-600	0.1–0.2
Test G (Cu-Al)	160	22.4	800–900-1000	150–275-400	0.1–0.2
Test H (Cu-Al)	420	58.8	700–850-1000	150–325-500	0.1–0.2

Fig. 3 Description of wobbling strategy

Table 4 Wobbling parameters

Wobbling thickness (t_h) [mm]	Tangential speed (V_t) [mm/s]	Wobbling frequency (f) [Hz]	Welding speed (V_f) [mm/s]	Wobbling overlap (O%) [%]
0.1	100	318	22.3	30
0.1	150	477	33.4	30
0.1	275	875	61.3	30
0.1	325	1034	72.4	30
0.1	350	1114	78.0	30
0.1	375	1194	83.6	30
0.1	400	1273	89.1	30
0.1	500	1591	111.4	30
0.1	600	1910	133.7	30
0.2	100	159	22.3	30
0.2	150	239	33.4	30
0.2	275	438	61.3	30
0.2	325	517	72.4	30
0.2	350	557	78.0	30
0.2	375	597	83.6	30
0.2	400	637	89.1	30
0.2	500	796	111.4	30
0.2	600	955	133.7	30
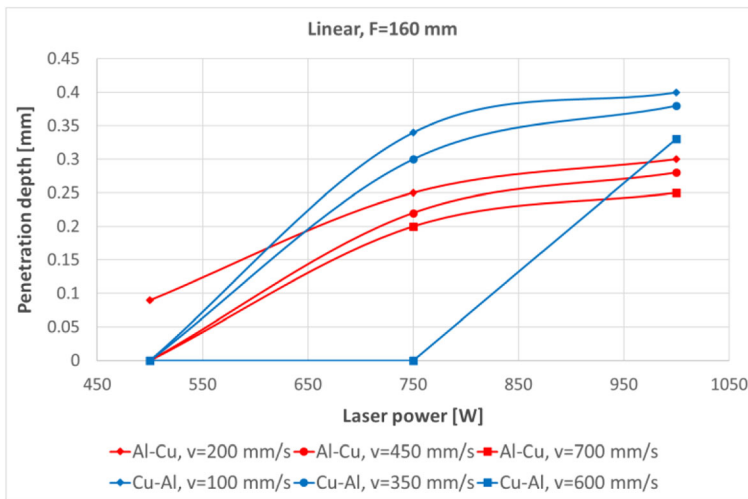
Fig. 4 Penetration depth, linear strategy, F = 160 mm (experiments A and E in Table 2)

a 160 mm focal length is exploited. Considering the nominal thickness of the metal sheets, 0.3 mm (Cu) and 0.4 mm (Al), it is immediately clear that the process parameters exploited lead to very different results, from no joining at all to complete cutting of the specimens (this aspect will be better clarified in section 3.4, where process windows are defined). These results are shown in Figs. 6 and 7, where significant micrographs are reported in order to have a visual correspondence of the four basic results: no joining, partial penetration, full penetration and complete cutting. Those micrographs also point out the different weld bead morphology characteristic of Al-Cu and Cu-Al configurations. In the first case the weld bead tends to be larger at the top and narrower at the bottom, while in the second one the situation is the opposite. This is due to the different physical characteristics of the two metals involved,
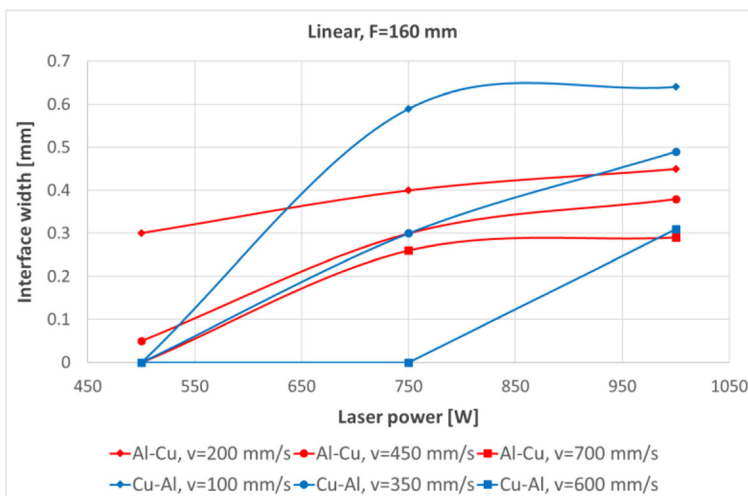

Fig. 5 Interface width, linear strategy, F = 160 mm (experiments A and E in Table 2)
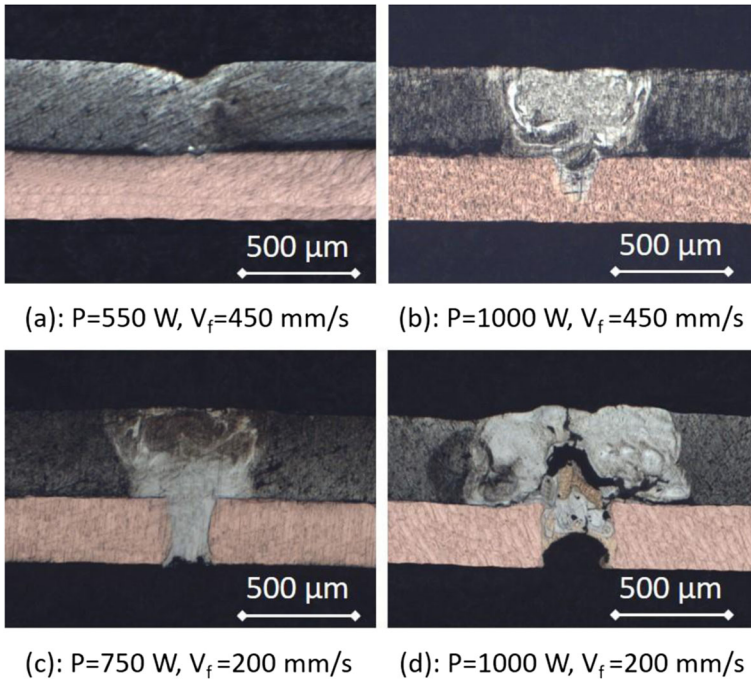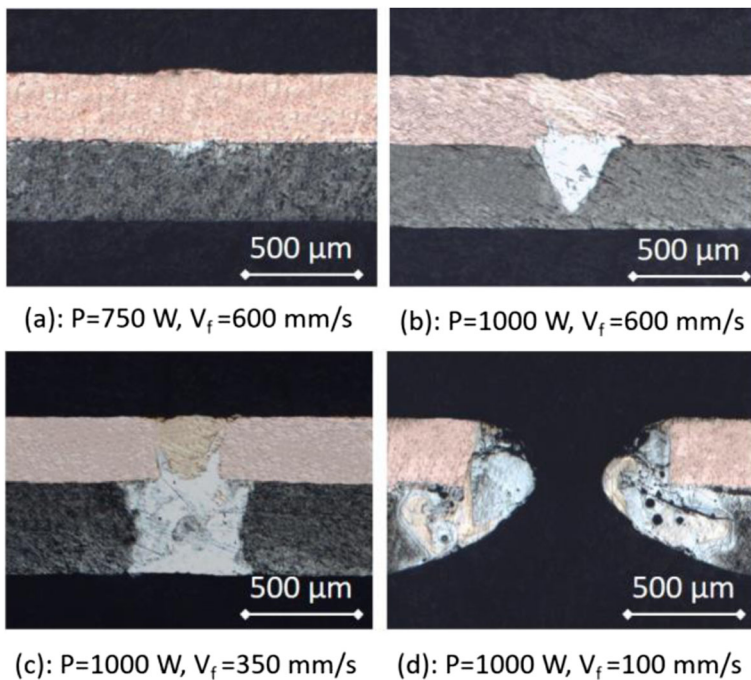
Fig. 6 Micrographs, linear strategy, F = 160 mm, Al-Cu

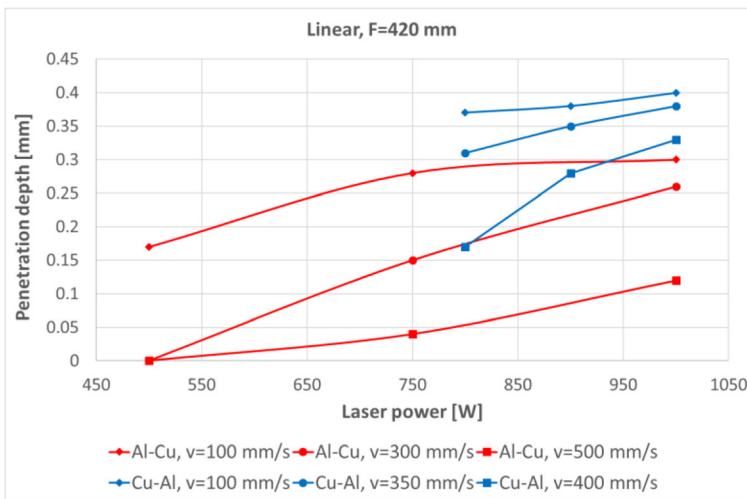**Fig. 7** Micrographs, linear strategy, F = 160 mm, Cu-Al

Fig. 8 Penetration depth, linear strategy, F = 420 mm (experiments B and F in Table 2)

particularly in terms of heat conduction coefficient and melting temperature. When the aluminum is at the top side, the laser beam melts the lower melting point material first and at the interface between the sheets the copper, which has a much higher melting point and a higher thermal conductivity than aluminum, melts to a much lower extent. When copper is at the top side, on the other hand, at the interface between the sheets it transfers heat very quickly, because of the higher melting temperature, to the aluminum, which melts abruptly and tends to favour a complete cutting of the specimen if the energy is excessive. This phenomenon is emphasized also by the lower absorptivity with respect to the laser radiation typical of copper (especially at the solid state). This characteristic implies, in fact, a high laser power required to trigger the melting of the first layers of the material and promote the formation of the keyhole. When the copper
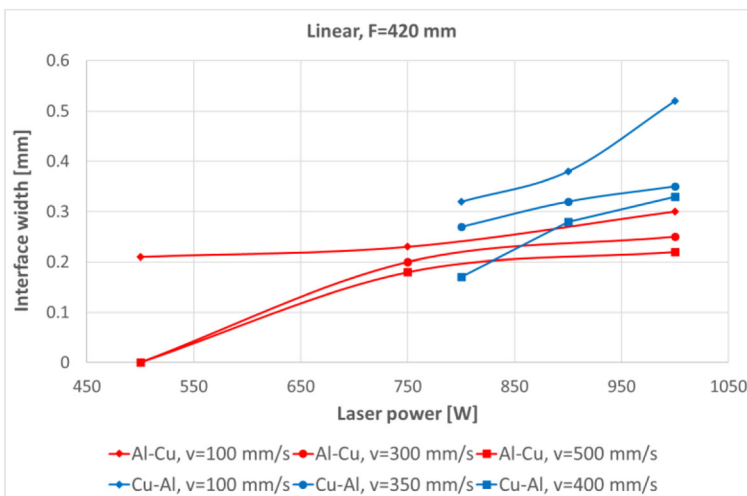

Fig. 9 Interface width, linear strategy, F = 420 mm (experiments B and F in Table 2)
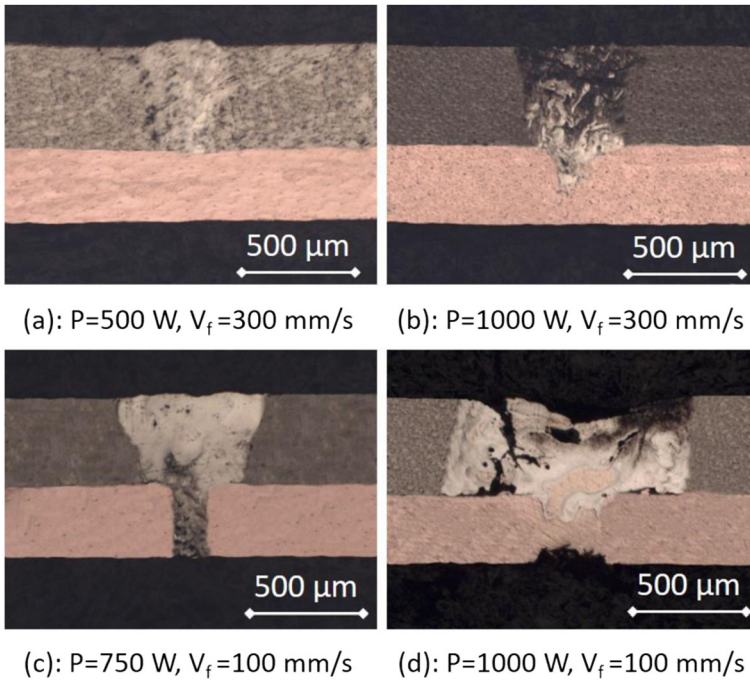
(a): P=500 W, V_f =300 mm/s   (b): P=1000 W, V_f =300 mm/s

(c): P=750 W, V_f =100 mm/s   (d): P=1000 W, V_f =100 mm/s

Fig. 10 Micrographs, linear strategy, F = 420 mm, Al-Cu

(a): P=800 W, V_f =400 mm/s   (b): P=900 W, V_f =100 mm/s

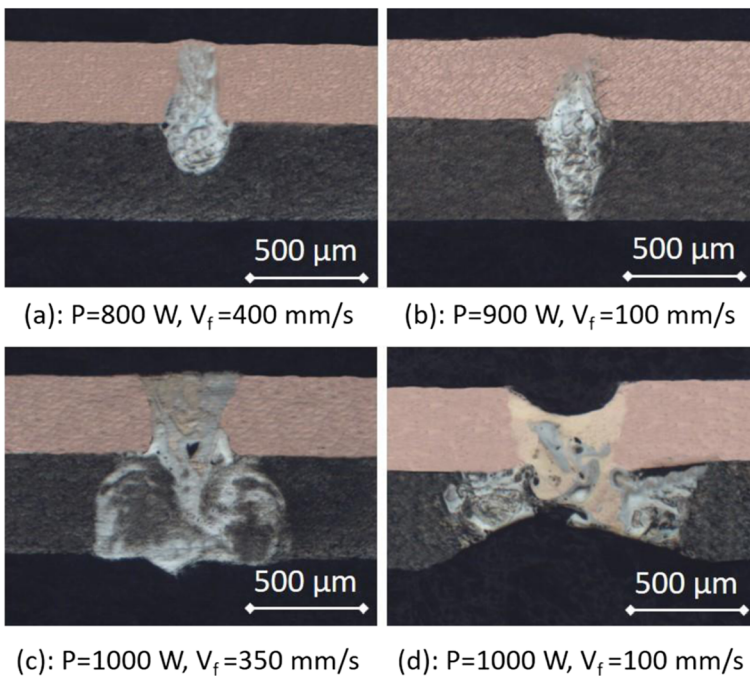(c): P=1000 W, V_f =350 mm/s   (d): P=1000 W, V_f =100 mm/s

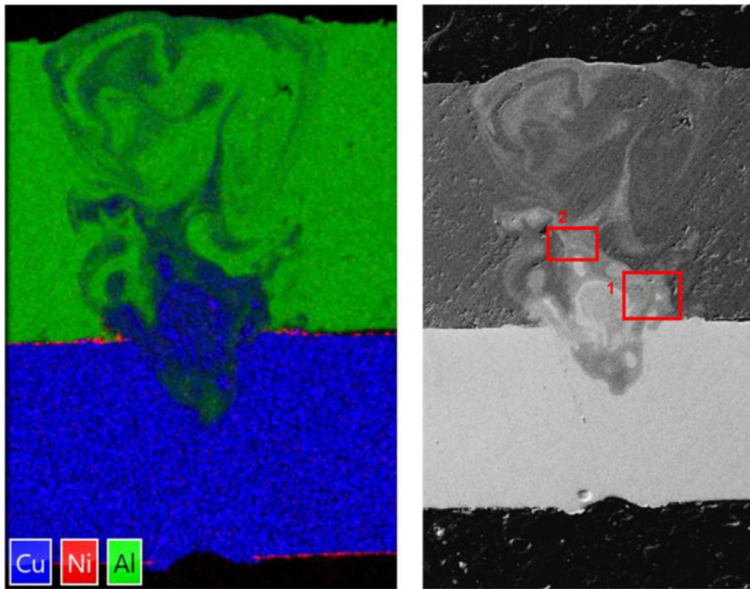**Fig. 11** Micrographs, linear strategy, F = 420 mm, Cu-Al

Fig. 12 SEM-EDS images obtained for partial penetration (Al-Cu), F = 160 mm

exceeds the melting point (and the keyhole eventually is formed), the absorptivity ramps up very quickly causing an abrupt overheating of the liquid phase, which, in turn, transfers this heat in excess to the bottom layer (aluminum).

Figures 8 and 9 show the variation of the weld bead dimensional characteristics with respect to process parameters and joint configuration when a 420 mm focal length is exploited. The larger spot characteristic of this configuration caused a reduction of the maximum welding speed from 700 mm/s to 500 mm/s, as well as a reduction of bead width at the interface and penetration depth for the same laser power and scanning speed. On the other hand, a larger focal length made the process less sensitive to the precision with which the workpiece was positioned in the focal plane, as the theoretical Rayleigh length switched from 0.3 mm to 2.2 mm.
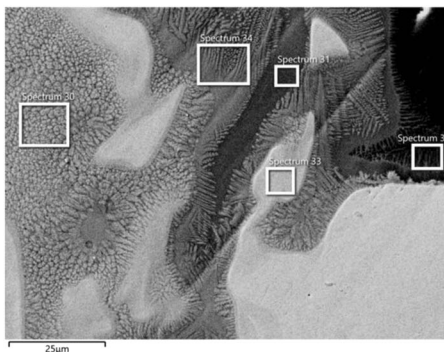
Wt.%	Al	Si	Fe	Ni	Cu	Total
Spectrum 30	36,05	0,03	0,2	0,27	63,45	100
Spectrum 31	71,55	0,07	0,27	0,06	28,05	100
Spectrum 32	86,53	0,06	0,26	2,55	10,6	100
Spectrum 33	11,47	0,1	0,15	0,42	87,87	100
Spectrum 34	53,18	0,12	0,22	0,23	46,24	100

Fig. 13 Composition investigation at the interface (Al-Cu), F = 160 mm
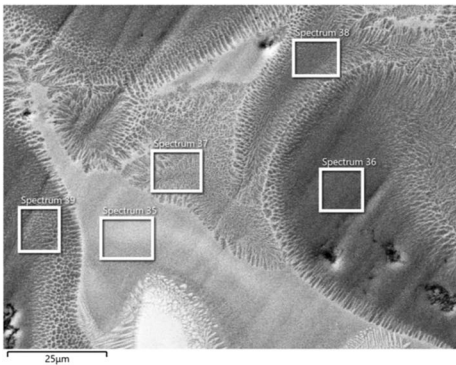
Wt.%	Al	Si	Fe	Ni	Cu	Total
Spectrum 35	63,49	0,09	0,22	0,38	35,82	100
Spectrum 36	97,86	0,03	0,33	0,03	1,74	100
Spectrum 37	74,91	0,02	0,29	0,21	24,57	100
Spectrum 38	90,75	0,04	0,22	0,13	8,85	100
Spectrum 39	90,26	0,06	0,29	0,31	9,08	100

Fig. 14 Composition investigation in zone 2 (Al-Cu), F = 160 mm

Figures 10 and 11 show some representative micrographs of this second batch of experimental trials: the weld bead morphology is very similar to the one described before.

The Cu-Al configuration with a 420 mm focal-length lens required absolutely the highest laser power, reducing the range of process parameters available to obtain good quality weld beads. The higher thermal conductivity and melting point of copper, together with the larger spot size, resulted in the need for higher specific energies to melt the copper layer. When penetration reached the interface, the aluminum foil, characterized by a much lower melting temperature, quickly overheated and abruptly melted. This made it much more difficult to accurately control penetration of the weld bead in the aluminum layer.

Figure 12 shows a representative example of resolidification after welding of a partial penetration joint in an Al-Cu configuration with a 160 mm focal-length lens. The image highlights the fact that welding takes place in a key-hole mode, with stirring
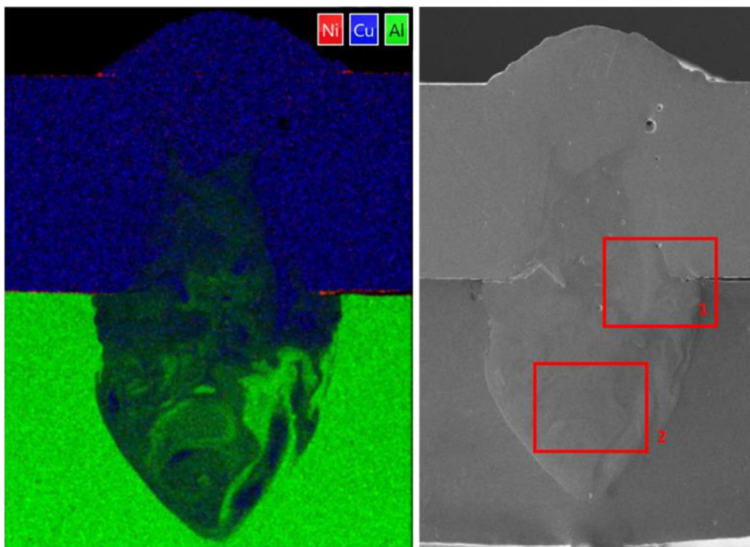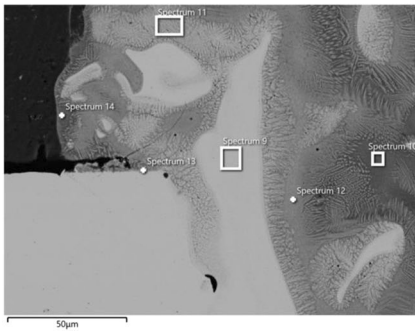

Fig. 15 SEM-EDS images obtained for partial penetration (Cu-Al), F = 160 mm

Wt. %	Al	Si	P	Fe	Ni	Cu	Total
Spectrum 9	7,74	0,05	0,03	0,12	0,01	92,05	100
Spectrum 10	62,88	0,07	0,05	0,26	0,28	36,47	100
Spectrum 11	31,15	0,03	0,09	0,22	0,79	67,72	100
Spectrum 12	40,24	0,05	0,1	0,09	0,43	59,09	100
Spectrum 13	39,06	0,05	2,29	0,2	7,43	50,97	100
Spectrum 14	62,53	0,11	0,04	0,16	0,65	36,53	100

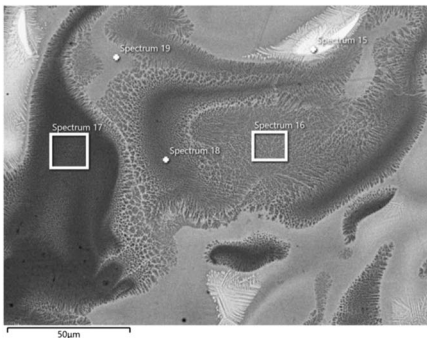| Atomic %	Al	Si	P	Fe	Ni	Cu	Total
Spectrum 9	16,48	0,09	0,05	0,12	0,01	83,23	100
Spectrum 10	79,87	0,08	0,06	0,16	0,16	19,67	100
Spectrum 11	51,5	0,05	0,13	0,18	0,6	47,54	100
Spectrum 12	61,24	0,07	0,13	0,07	0,3	38,19	100
Spectrum 13	58,95	0,07	3,02	0,14	5,15	32,67	100
Spectrum 14	79,61	0,13	0,04	0,1	0,38	19,75	100

Fig. 16 Composition investigation at the interface (Cu-Al), F = 160 mm

effects taking place due to formation of high-pressure metal vapor, dragging part of the molten copper pool upwards into the aluminum pool. The nickel coating, visible as a thin red layer in the same figure, is completely dispersed in the melted zone due to partial evaporation and mixing with the parent materials.

In order to investigate the composition of the fused zone, significant welded samples were analyzed in two different areas of the melted zone; near the interface (rectangle 1 in Fig. 12) and far from the interface in the high-dilution zone that is confined, in this case, to the upper aluminum melt pool (rectangle 2 in Fig. 12). Local compositions are reported in Figs. 13 and 14.

Figure 15 is representative of Cu-Al joints obtained with a 160 mm focal-length lens and characterized by partial penetration. The welding mode is once again key-hole but mixing of the two base materials is different from the case presented in Fig. 12. The higher-density copper tends to diffuse downwards into the aluminum melt pool and thus the high dilution zone is shifted into the lower sheet. For this reason, EDS analyses were performed in the interface zone (rectangle 1 in Fig. 15) and the bottom zone (rectangle 2 in Fig. 15).

Figure 16 shows that considerable mixing of the two metals takes place at the interface, with consequent possible formation of hard and brittle intermetallic compounds. From analysis of Fig. 17, it can be seen that these compounds can also be present at the root of the weld bead. The composition analysis carried out in this study was aimed at understanding the preferential distributions of the alloying elements in the

Wt. %	Al	Si	Fe	Ni	Cu	Total
Spectrum 15	25,63	0,04	0,13	0,24	73,97	100
Spectrum 16	72,21	0,06	0,28	0,3	27,15	100
Spectrum 17	94,06	0,03	0,29	0,07	5,55	100
Spectrum 18	83,29	0,05	0,27	0,2	16,19	100
Spectrum 19	64,88	0,07	0,27	0,33	34,45	100

Atomic %	Al	Si	Fe	Ni	Cu	Total
Spectrum 15	44,77	0,06	0,11	0,19	54,87	100
Spectrum 16	85,89	0,07	0,16	0,16	13,71	100
Spectrum 17	97,35	0,03	0,15	0,03	2,44	100
Spectrum 18	92,1	0,06	0,14	0,1	7,6	100
Spectrum 19	81,24	0,08	0,16	0,19	18,32	100

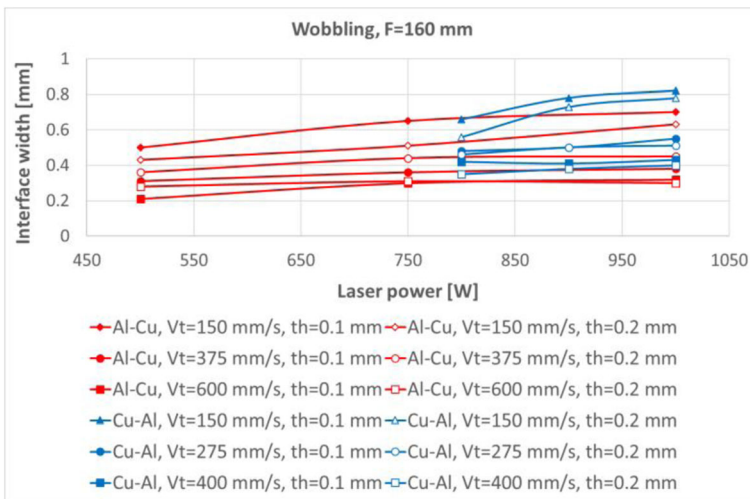**Fig. 17** Composition investigation in zone 2 (Cu-Al), F = 160 mm

Fig. 18 Interface width, wobbling strategy, F = 160 mm (experiments C and G in Table 2)

weld beads and not to determining the exact intermetallic phases occurring in the different portions of the molten pool.

Morphology and Microstructure in Welding with Wobbling Scanning Strategy

Figure 18 presents the weld bead width at the interface in an Al-Cu and Cu-Al configuration with a 160 mm focal-length lens using a wobbling beam scanning strategy. The graph points out that weld bead width is much more influenced by tangential welding speed than laser power. Concerning weld penetration depth all the trials showed full penetration or complete cutting, thus non graphs concerning this parameter are shown in this section. This result puts in evidence that wobbling strategy
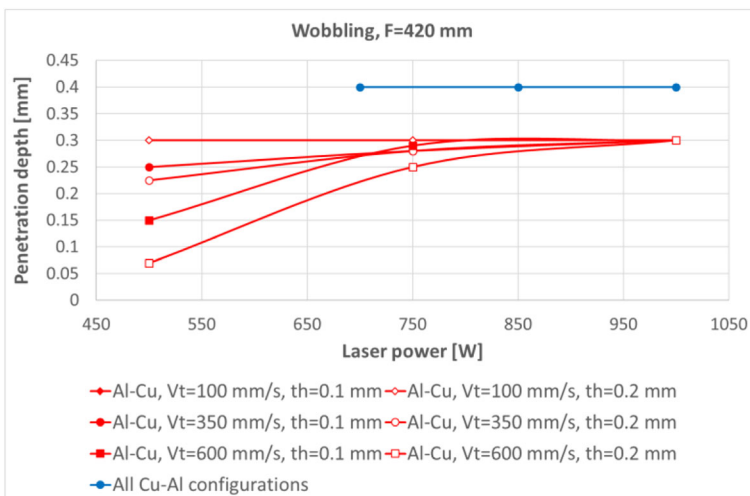

Fig. 19 Penetration depth, wobbling strategy, F = 420 mm (experiments D and H in Table 2)
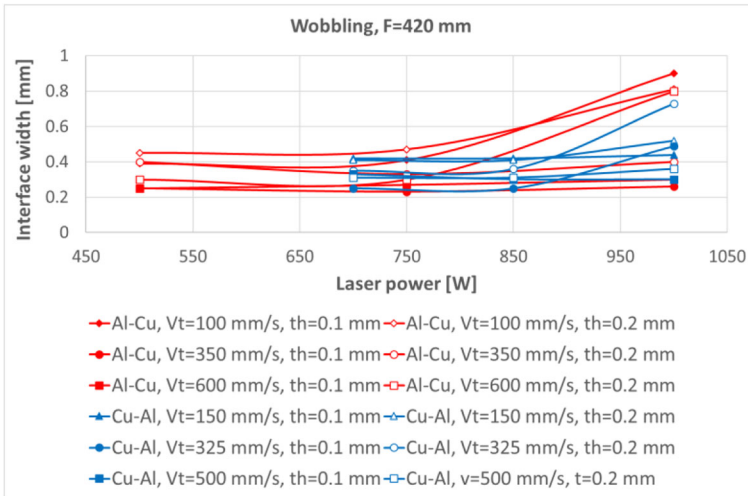
Fig. 20 Interface width, wobbling strategy, F = 420 mm (experiments D and H in Table 2)

associated to a very small spot leads to a very difficult control of the heat input in the weld bead.
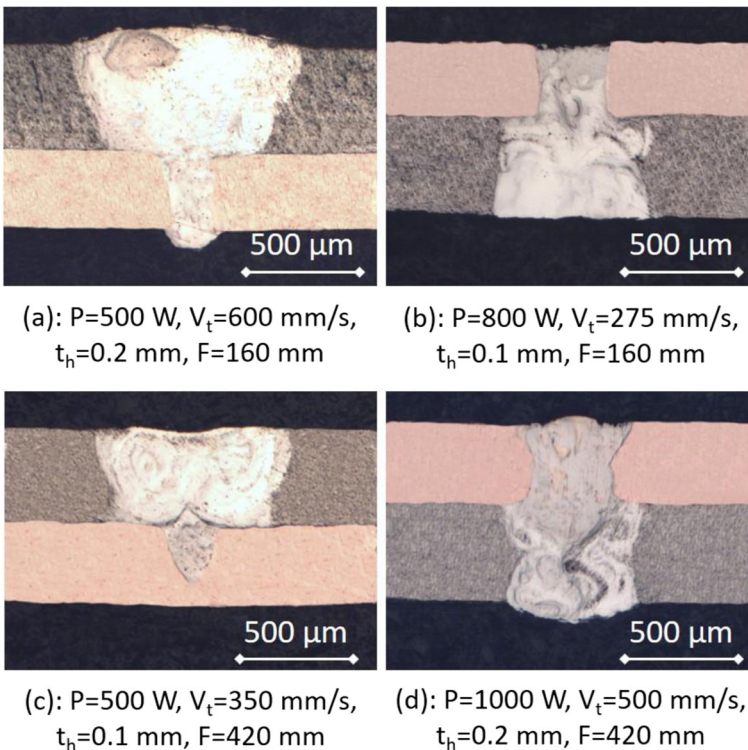

(a): P=500 W, V_t=600 mm/s, t_h=0.2 mm, F=160 mm

(b): P=800 W, V_t=275 mm/s, t_h=0.1 mm, F=160 mm

(c): P=500 W, V_t=350 mm/s, t_h=0.1 mm, F=420 mm

(d): P=1000 W, V_t=500 mm/s, t_h=0.2 mm, F=420 mm

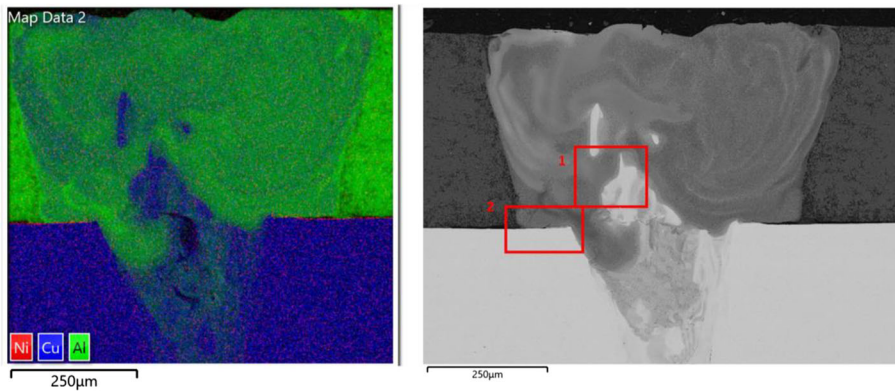Fig. 21 Micrographs, wobbling strategy

**Fig. 22** SEM-EDS images with wobbling strategy (Cu-Al), F = 420 mm

Figures 19 and 20 show the results achieved by means of the 420 mm focal length lens: in this case it was possible to obtain joints with partial penetration and interface widths similar to those seen with a linear scanning strategy, especially at lower laser power. These trends were also confirmed by optical microscopy (Fig. 21).

Concerning Cu-Al configuration, in particular, the higher melting temperature of copper layer firstly lead to higher power requirements compared to the Al-Cu one. Moreover, the higher power requirements result in a large aluminum weld pool for both focal lengths as seen in Fig. 21.

The SEM-EDS analysis presented in Fig. 22 confirms the presence of large areas of mixture of the two base materials not only at the interface, but also within the rest of the molten zone. This is especially true in an Al-Cu configuration, where results are similar to the ones concerning the linear scanning strategy. Once again, in this case, a reduction in specific energy with lower power or higher welding speed lead to a decrease in the extension of these zones. Local compositions of intermetallic compounds are reported in Figs. 23 and 24.

Shear Test Results

Shear tests were performed by means of an Instron 8032 machine equipped with a 2 kN load cell. A schematic of the shear test is presented in Fig. 25. Figure 26 presents the maximum measured shear loads for the different experiments in an Al-Cu configuration, both with linear and wobbling scanning strategies, as a function of the weld bead
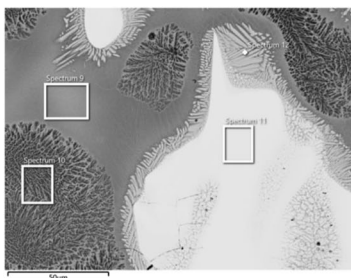
Wt. %	Al	Si	Fe	Ni	Cu	Total
Spectrum 9	63,41	0,07	0,26	0,14	36,11	100
Spectrum 10	77,36	0,06	0,21	0,05	22,32	100
Spectrum 11	11,14	0	0,08	0,27	88,51	100
Spectrum 12	51,04	0,07	0,16	0,11	48,63	100

Atomic %	Al	Si	Fe	Ni	Cu	Total
Spectrum 9	80,26	0,09	0,16	0,08	19,41	100
Spectrum 10	88,9	0,07	0,12	0,03	10,89	100
Spectrum 11	22,78	0	0,08	0,25	76,89	100
Spectrum 12	71,01	0,09	0,11	0,07	28,73	100

Fig. 23 Composition investigation at the interface in zone 1 (Al-Cu), F = 420 mm
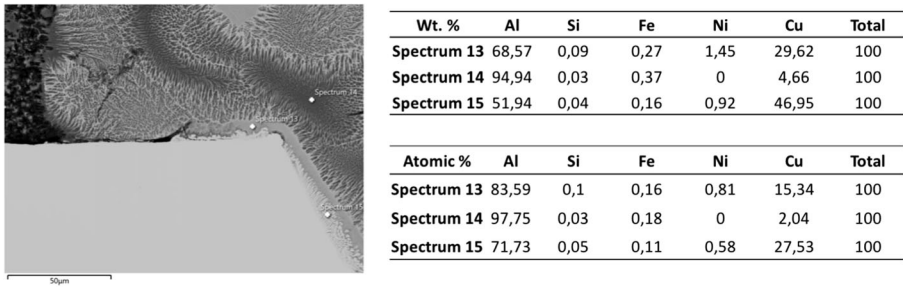
Wt. %	Al	Si	Fe	Ni	Cu	Total
Spectrum 13	68,57	0,09	0,27	1,45	29,62	100
Spectrum 14	94,94	0,03	0,37	0	4,66	100
Spectrum 15	51,94	0,04	0,16	0,92	46,95	100

Atomic %	Al	Si	Fe	Ni	Cu	Total
Spectrum 13	83,59	0,1	0,16	0,81	15,34	100
Spectrum 14	97,75	0,03	0,18	0	2,04	100
Spectrum 15	71,73	0,05	0,11	0,58	27,53	100

Fig. 24 Composition investigation at the interface in zone 2 (Al-Cu), F = 420 mm

width at the interface. For every batch of experiments (A, B, C and D) the specimens characterized by a visually sound weld bead were subjected to shear test and the results were aggregated as a function of the width of the weld bead at the interface between the two sheets.

The results highlight a number of important aspects. Firstly, the maximum strength is achieved with both scanning strategies in correspondence to a width of the interface between the sheets in the range 0.2–0.3 mm. Widths at interface smaller than 0.2 mm lead to insufficient strength while widths larger than 0.3 mm provoke a decrease in strength due to the thermal degradation of the characteristics of the materials and to the formation of more intermetallic compounds. Moreover, a linear scanning strategy
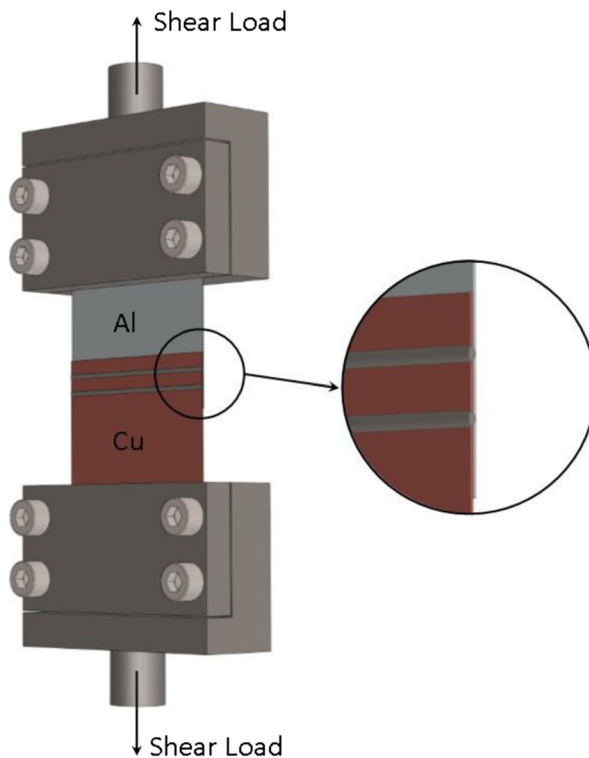

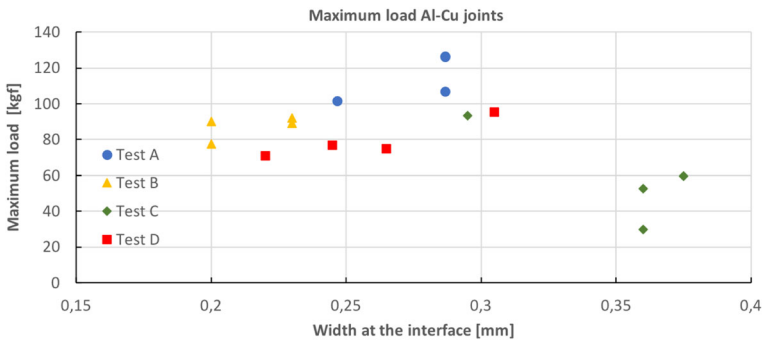**Fig. 25** Schematic of shear test

Fig. 26 Shear tests: maximum load (Al-Cu)

(Tests A and B) lead to a higher average shear strength than a wobbling one, for the same width at the interface. Finally, the wobbling strategy always delivers more energy to the target than the linear strategy. This last consideration demonstrates that temperatures reached by the specimens were higher and cooling speeds were lower than the ones registered in case of linear scanning strategy. These conditions promote the formation of a greater quantity of intermetallic compounds and make the weld bead less resistant, in accordance with the results explained in [16].

Figure 27 summarizes the shear test results obtained in a Cu-Al configuration: the data are aggregated similarly to the ones described in Fig. 26. It is once again evident that the linear scanning strategy produces weld beads with higher average shear strength than the wobbling strategy for the same width at the interface. From these results it is not possible to define an optimum width which maximizes the mechanical resistance of the joint, but it can be stated that relatively large weld beads produce weaker joints due to increased formation of intermetallic compounds.

Figure 28 presents maximum loads as a function of the number of weld beads per joint for all of the considered configurations. The presented data are average values obtained with 10 specimens for all configurations, starting from the process parameter configuration that led to maximum strength for each number of beads. The results show that switching from a 1- to 2-bead configuration causes an increase in the maximum load approximately equal to 20%, except in the case of a wobbling strategy and Cu-Al
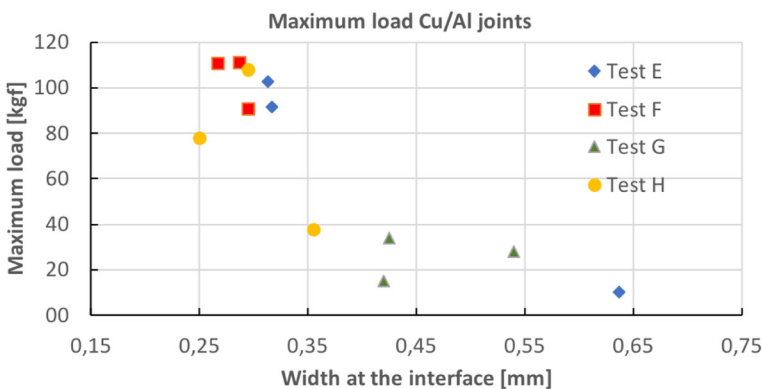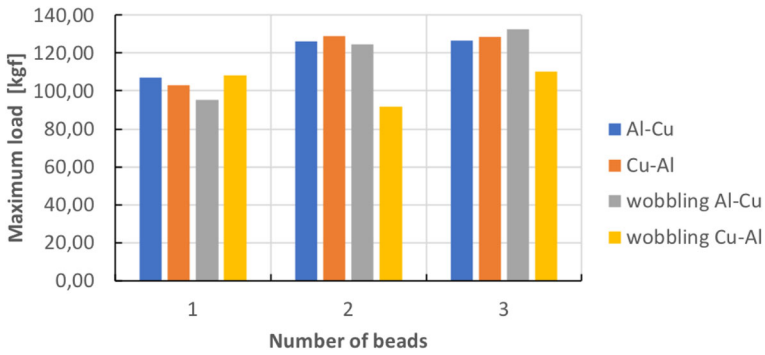

Fig. 27 Shear tests: maximum load (Cu-Al)

Fig. 28 Maximum load (all configurations)

configuration where the reduction is around 15%. Switching from a 2- to 3-bead configuration causes a negligible increase in strength with a wobbling strategy (approximately 5%), while such an increase is not evident using a linear strategy.

Process Windows Definition

The last analysis carried out in this work concerned the definition of process windows for the different configurations. In the definition of the tables in Figs. 29 and 30 a colour map was used in order to visually define the different cases occurred: no joining (blue), partial penetration (green), full penetration (yellow) and complete cutting or severe damage of the bead (red). Figure 29 shows process windows related to linear strategy: it is clear that in Cu-Al configuration the possibility to achieve a partial penetration is more difficult than in Al-Cu one.

Figure 30 shows process windows related to wobbling strategy: in this case the higher energy involved makes the process more difficult to be fine tuned and an accurate control of penetration depth is hardly achievable.

Conclusions

This paper deals with laser lap-welding of thin aluminum and copper sheets in both Al-Cu and Cu-Al configurations. Specifically, morphological, metallurgical and
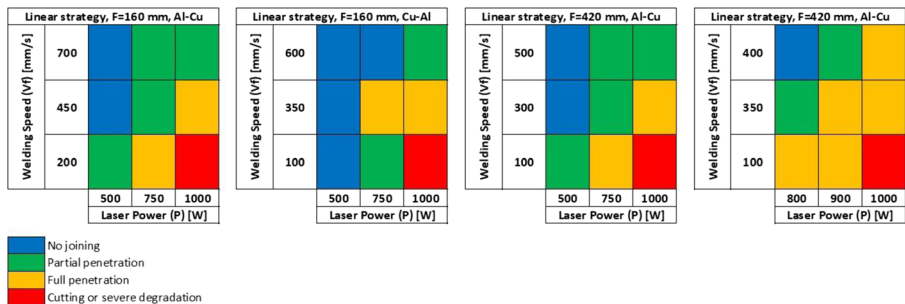

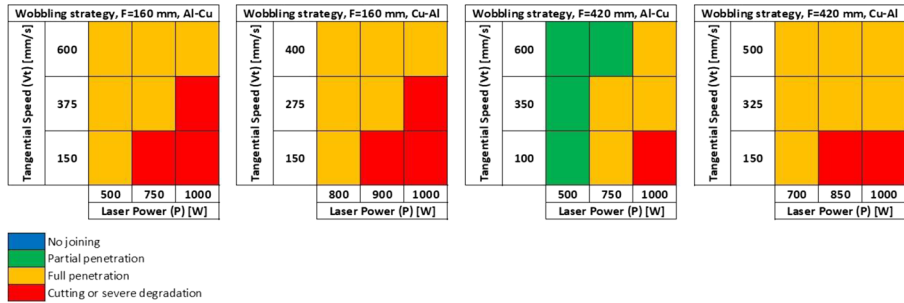**Fig. 29** Process windows, linear scanning strategy

Fig. 30 Process windows, wobbling scanning strategy

mechanical tests were carried out to determine optimum process windows. Linear and wobbling beam scanning strategies were investigated varying the laser power, welding speed and spot diameter. In relation to the tested variables, which were repeated for both Al-Cu and Cu-Al configurations, the following results were found:

- A linear scanning strategy tends to give higher maximum loads for the same energy density compared to a wobbling scanning strategy.
- The use of a 160 mm focal length lens does not allow to achieve good results in the case of wobbling strategy due to the high energy density for either Al-Cu and Cu-Al configurations. On the other hand, strong sound joints were obtained in both configurations with a 420 mm focal length lens.
- Switching from a 1- to 2-bead configuration yielded a 20% increase in joint strength, while switching from a 2- to 3-bead configuration led to negligible increases.
- SEM EDS analysis revealed a strong mixing of the two metals in the fused zone for all investigated process parameters and thus the formation of intermetallics is highly promoted.
- Both linear and wobbling beam scanning strategies allowed to generate sound joints, characterized by a maximum tensile load up to 130 kg.
- The exploitation of a high brilliance single laser source made it possible to investigate all the configurations described in this work and allowed to keep the heat input in the weld bead very low. The results achieved with the wobbling technique allow to conclude that sound joints could be achieved also by means of a lower quality laser source.

References

1. Albright, C.E.: The fracture toughness testing of steel-aluminum deformation welds. Eng. Fract. Mech. **15**(1–2), 193–203 (1981). https://doi.org/10.1016/0013-7944(81)90117-X

2. Date, H., Kobayakawa, S., Naka, M.: Microstructure and bonding strength of impact-welded aluminium–stainless steel joints. J. Mater. Process. Technol. **85**(1–3), 166–170 (1999). https://doi.org/10.1016/S0924-0136(98)00284-2

3. Fukumoto, S., Tsubakino, H., Okita, K., Aritoshi, M., Tomita, T.: Amorphization by friction welding between 5052 aluminum alloy and 304 stainless steel. Scr. Mater. **42**(8), 807–812 (2000). https://doi.org/10.1016/S1359-6462(00)00299-2

4. Lee, W.B., Schmuecker, M., Mercardo, U.A., Biallas, G., Jung, S.B.: Interfacial reaction in steel–aluminium joints made by friction stir welding. Scr. Mater. **55**(4), 355–358 (2006). https://doi.org/10.1016/j.scriptamat.2006.04.028

5. Sierra, G., Peyre, P., Deschaux-Beaume, F., Stuart, D., Fras, G.: Steel to aluminium key-hole laser welding. Mater. Sci. Eng. A. **447**(1–2), 197–208 (2007). https://doi.org/10.1016/j.msea.2006.10.106

6. Mai, T.A., Spowage, A.C.: Characterisation of dissimilar joints in laser welding of steel–kovar, copper–steel and copper–aluminium. Mater. Sci. Eng. A. **374**(1–2), 224–233 (2004). https://doi.org/10.1016/j.msea.2004.02.025

7. Abbasi, M., Karimi Taheri, A., Salehi, M.T.: Growth rate of intermetallic compounds in Al/cu bimetal produced by cold roll welding process. J. Alloys Compd. **319**(1–2), 233–241 (2001). https://doi.org/10.1016/S0925-8388(01)00872-6

8. Lee, W.B., Bang, K.S., Jung, S.B.: Effects of intermetallic compound on the electrical and mechanical properties of friction welded cu/Al bimetallic joints during annealing. J. Alloys Compd. **390**(1–2), 212–219 (2005). https://doi.org/10.1016/j.jallcom.2004.07.057

9. Panaskar, N., Terkar, R.: A review on recent advances in friction stir lap welding of Aluminium and copper. Mater. Today. **4**(8), 8387–8393 (2017). https://doi.org/10.1016/j.matpr.2017.07.182

10. Wei, Y., Li, J., Xiong, J., Zhang, F.: Investigation of interdiffusion and intermetallic compounds in Al–cu joint produced by continuous drive friction welding. Engr. Sci. Tech. **19**(1), 90–95 (2016). https://doi.org/10.1016/j.jestch.2015.05.009

11. Fei, X., Ye, Y., Jin, L., Wang, H., Lv, S.: Special welding parameters study on cu/Al joint in laser-heated friction stir welding. J. Mater. Process. Technol. **256**, 160–171 (2018). https://doi.org/10.1016/j.jmatprotec.2018.02.004

12. Raoelison, R.N., Sapanathan, T., Buiron, N., Rachik, N.: Magnetic pulse welding of Al/Al and Al/cu metal pairs: consequences of the dissimilar combination on the interfacial behavior during the welding process. J. Manuf. Process. **20**(1), 112–127 (2015). https://doi.org/10.1016/j.jmapro.2015.09.003

13. Fujii, H.T., Endo, H., Sato, Y.S., Kokawa, H.: Interfacial microstructure evolution and weld formation during ultrasonic welding of Al alloy to cu. Mater. Charact. **139**, 233–240 (2018). https://doi.org/10.1016/j.matchar.2018.03.010

14. Weigl M, Albert F, Schmidt M. Enhancing the ductility of laser-welded copper-aluminum connections by using adapted filler materials. Phys. Procedia 2011;12(B):332–338. https://doi.org/10.1016/j.phpro.2011.03.141

15. Solchenbach, T., Plapper, P.: Mechanical characteristics of laser braze-welded aluminium–copper connections. Opt. Laser Technol. **54**, 249–256 (2013). https://doi.org/10.1016/j.optlastec.2013.06.003

16. Lee, S.J., Nakamura, H., Kawahito, Y., Katayama, S.: Effect of welding speed on microstructural and mechanical properties of laser lap weld joints in dissimilar Al and cu sheets. Sci. Technol. Weld. Join. **19**(2), 111–118 (2014). https://doi.org/10.1179/1362171813Y.0000000168

17. Zuo, D., Hu, S., Shen, J., Xue, Z.: Intermediate layer characterization and fracture behavior of laser-welded copper/aluminum metal joints. Mater. Des. **58**, 357–362 (2014). https://doi.org/10.1016/j.matdes.2014.02.004

18. Stritt, P., Hagenlocher, C., Kizler, C., Weber, R., Rüttimann, C., Graf, T.: Laser spot welding of copper-aluminum joints using a pulsed dual wavelength laser at 532 and 1064nm. Phys. Procedia. **56**, 759–767 (2014). https://doi.org/10.1016/j.phpro.2014.08.083

19. Fetzer, F., Jarwitz, M., Stritt, P., Weber, R., Graf, T.: Fine-tuned remote laser welding of aluminum to copper with local beam oscillation. Phys. Procedia. **83**, 455–462 (2016). https://doi.org/10.1016/j.phpro.2016.08.047

20. Schmalen, P., Plapper, P., Peral, I., Titov, I., Vallcorba, O., Rius, J.: Composition and phases in laser welded Al-cu joints by synchrotron x-ray microdiffraction. Procedia CIRP. **74**, 27–32 (2018). https://doi.org/10.1016/j.procir.2018.08.006

21. Reisgen, U., Olschok, S., Jakobs, S., Holtum, N.: Influence of the degree of dilution with laser beam vacuum-welded cu-Al mixed joints on the electrical properties. Procedia CIRP. **74**, 23–26 (2018). https://doi.org/10.1016/j.procir.2018.08.022

22. Kermanidis, T., Christodoulou, P.I., Hontzopoulos, E., Haidemenopoulos, G.N., Kamoutsi, H., Zervaki, A.D.: Mechanical performance of laser spot-welded joints in Al-Al/cu solar thermal absorbers. Mater. Des. **155**, 148–160 (2018). https://doi.org/10.1016/j.matdes.2018.05.052

Publisher's Note   Springer Nature remains neutral with regard to jurisdictional claims in published maps and institutional affiliations.